Study of Josephson Generation Harmonics in a Long Josephson Junction

Kinev, N. V.; Rudakov, K. I.; Filippenko, L. V.; Koshelets, V. P.

Published in:
Radiophysics and quantum electronics

DOI:
10.1007/s11141-023-10240-4

Publication date:
2023

DOI 10.1007/s11141-023-10240-4
Radiophysics and Quantum Electronics, Vol. 65, No. 8, January, 2023
(Russian Original Vol. 65, No. 8, August, 2022)

STUDY OF JOSEPHSON GENERATION HARMONICS IN A LONG JOSEPHSON JUNCTION

N. V. Kinev,[1] * **K. I. Rudakov,**[2] **L. V. Filippenko,**[1] **and V. P. Koshelets** [1]

UDC 537.862

We present the results of experimental study of the harmonics of Josephson radiation from a terahertz (THz) source based on a long Josephson junction (LJJ). The source consists of an integrated circuit including the LJJ, a matched transmitting antenna, and a harmonic mixer used for phase locking of the output signal. The LJJ and the harmonic mixer are both made of three-layer Nb-AlOx-Nb superconductor–insulator–superconductor (SIS) structures and operate at a temperature of 4.2 K. The antenna is located in the base superconducting Nb electrode of the microcircuit. To study the spectral composition and characteristics of the output radiation, two different methods were employed, using a THz Fourier transform spectrometer based on a broadband semiconductor detector and using a high-resolution THz spectrometer based on a heterodyne SIS receiver. The spectral composition of the radiation demonstrates the presence of both the fundamental harmonic of the Josephson effect and the higher harmonics. The spectral characteristics of the fundamental (at frequencies of 300–335 *GHz) and the second (at frequencies of* 600–670 *GHz) harmonics, respectively, with a spectral resolution of about 0.1 MHz were studied using a SIS detector.*

1. INTRODUCTION

The nonstationary Josephson effect, discovered more than 50 years ago [1–4], is conventionally described by the following equation [2]:

$$\hbar \partial\varphi/\partial t = 2eV_{\mathrm{DC}}, \tag{1}$$

where $\hbar$ is the reduced Planck constant, φ is the phase difference between the sides of the Josephson contact, t is the time, e is the electron charge, and V_{DC} is the constant voltage at the contact. Equation (1) determines the fundamental frequency f_{J} of the Josephson generation as

$$f_{\mathrm{J}} = (2e/h)V_{\mathrm{DC}}. \tag{2}$$

The existence of harmonics with frequencies $f_N = N f_{\mathrm{J}}$, where N is a natural number greater than 2, was predicted and numerically described long ago in some simplified models of the Josephson junction (see, e. g., [5, 6]) and was also demonstrated indirectly based on the observation of some features of current–voltage characteristics (IVCs) [7]. In other papers, a similar effect, which consists in the generation of harmonics of an external microwave signal fed to the Josephson contact [8–10], was detected, i. e., the contact operated as a frequency multiplier. In this case, direct experimental observations of Josephson harmonics at the true generation frequency (not from measurements of IVC features) are still missing in the publications. The

* nickolay@hitech.cplire.ru

[1] V. A. Kotel'nikov Institute of Radio Engineering and Electronics of the Russian Academy of Sciences, Moscow, Russia; [2] Groningen University, Groningen, The Netherlands. Translated from Izvestiya Vysshikh Uchebnykh Zavedenii, Radiofizika, Vol. 65, No. 8, pp. 651–661, August 2022. Russian DOI: 10.52452/00213462_2022_65_08_651 Original article submitted May 6, 2022; accepted August 31, 2022.

reason is that the total output power of the Josephson junction is fairly low, from a few nanowatts to a few microwatts [4, 11], while the power of the higher harmonics is much less than that of the fundamental [6]. It should also be noted that there are no technical capabilities for stable measurement of such weak signals in the terahertz frequency range. The purpose of this work is to study directly the harmonics at the carrier (true) generation frequency.

In recent years, a Josephson terahertz source, which emits a signal into free space has been developed and comprehensively studied on the basis of the LJJ manufactured from Nb-AlO_x-Nb three-layer structures with a tunnel current density of 5–10 kA/cm^2 [12–18]. Radiation into free space is provided by a transmitting planar slot antenna which is matched with the LJJ on an integrated circuit and is located in the focus of a semi-elliptic silicon lens. This antenna is designed in a 200 nm layer of the lower electrode of the niobium microcircuit. The stabilization of the output radiation of the oscillator is successfully performed by a phase locking loop, which uses the signal of a harmonic mixer based on the superconductor–insulator–superconductor junction (SIS junction), located on a common integrated microcircuit in the feedback circuit. Various source microcircuit topologies of the form of a long Josephson junction+antenna+harmonic source have been developed and explored, jointly covering a frequency tuning range of 200 to 750 GHz [12–14]. To examine output radiation into free space, both its direct detection using a highly sensitive broadband and cooled to 4.2 K silicon-based bolometer and heterodyne detection using a superconducting integrated receiver (SIR) in the range 500–700 GHz based on an SIS mixer [19, 20] with a spectral resolution of about 0.1 MHz were employed. The SIR frequency operating range is not wide enough (about 35% of the center frequency) to observe two harmonics at frequencies f and $2f$ at the same time.

The first study of Josephson harmonics using the oscillator we developed has recently been presented by a group of authors in [18], where the presence of harmonics of the signal of a fundamental frequency of up to 280 GHz was demonstrated. In that work, a Nb-AlO_x-Nb junction with a length of 400 μm in the wave propagation direction was used as the LJJ. This junction length is optimal for operating frequencies above 400 GHz, where the Fiske steps (a resonant structure on the IVC due to reflections from the junction edges) are inclined enough to ensure continuous frequency tuning in a wide range. In turn, for operation at frequencies below 400 GHz, where the Fiske steps are almost vertical, continuous tuning can be achieved by increasing the junction length, which leads to a higher surface loss and, consequently, a greater step inclination. Therefore, in the present paper, new experimental samples with an operating range of first-harmonic output frequencies 250–400 GHz based on an LJJ having a length of 700 μm were additionally manufactured and examined. Also, generation spectra with a set of closely spaced fundamental harmonic frequencies in the range 300–325 GHz were studied to extend the results of [18]. In addition, a more detailed analysis of the causes of the appearance of artificial harmonics in the detected spectrum was performed.

The paper uses a broadband Fourier transform spectrometer with a detector based on a silicon bolometer to distinguish generation harmonics (Sec. 2). Then, after studying the harmonic composition, the amplitude–frequency characteristics (AFCs) of the first and second harmonics with high spectral resolution were examined, where the fundamental (first) harmonic was recorded using a feedback circuit to stabilize the source and the second harmonic, using an SIR (Sec. 3).

2. STUDY OF THE HARMONIC COMPOSITION USING A FOURIER TRANSFORM SPECTROMETER

The layout of the experimental setup for studying the harmonic composition of radiation is shown in Fig. 1. A Fourier transform spectrometer based on a Michelson interferometer with two mirrors and a beam splitter located at an angle of 45° to the incident signal is used. A broadband infrared commercially available silicon-based bolometer with a sensitivity of about $1.4 \cdot 10^{-13}$ W/Hz$^{1/2}$, which is cooled to 4.2 K, was used as a detector. The detector records the result of interference of two beams reflected from the movable and fixed mirrors, depending on the position of the movable mirror, after which the frequency spectrum of the original signal is reconstructed by using Fourier transform. The bolometer signal is recorded employing a synchronous amplifier with a signal modulation frequency of 170 Hz. The maximum spectral resolution δf

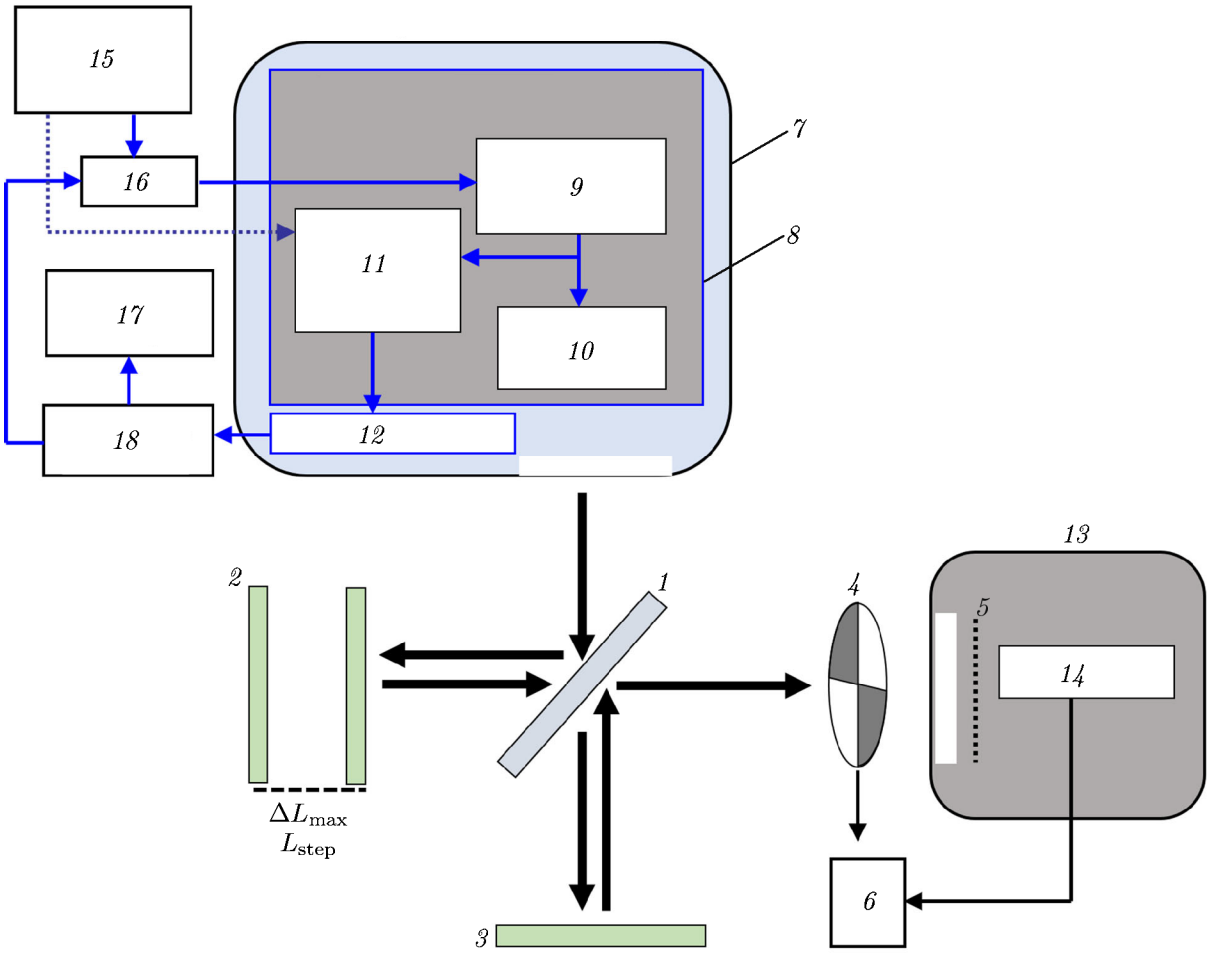

Fig. 1. Layout of the experimental setup of a Fourier transform spectrometer based on a Michelson interferometer for a study of the spectral composition of LJJ radiation: *1* is the beam splitter, *2* is the movable mirror, *3* is the fixed mirror, *4* is the optical interrupter, *5* is the input infrared filter, and *6* is the synchronous amplifier. Cryostat *7* includes integrated circuit *8* (*9* is an LJJ of the frequency range 250–700 GHz, *10* is the slot antenna, and *11* is the harmonic mixer) and intermediate frequency amplifier *12* and cryostat *13* includes bolometer *14*. The diagram also shows the reference microwave oscillators *15*, phase locking loop *16*, spectrum analyzer *17*, and intermediate frequency amplifier *18*.

of the spectrometer is determined as

$$\delta f \approx c/(2\,\Delta L_{\max}) = 0.75 \text{ GHz}, \tag{3}$$

where c is the speed of light and $\Delta L_{\max}$ is the maximum travel length of the movable mirror, which is 200 mm for the current experimental setup. Such a spectral resolution is excessive for the purposes of distinguishing harmonics that are several hundred gigahertz spaced; therefore, a travel length of 24 mm, which corresponds to a spectral resolution of 6.25 GHz, was used in the experiment. The maximum frequency of the recorded spectral characteristic $f_{\max}$, in turn, is determined by the minimum step L_{step} of the movable mirror, which is 2.5 μm in the stepper motor we used:

$$f_{\max} \approx c/(4\,L_{\text{step}}) = 30 \text{ THz}. \tag{4}$$

Equation (4) describes the perfect case and does not take into account the accuracy factor of spectrum reconstruction, which reduces the actual maximum frequency with a coefficient of about 1.00–1.25. As the maximum spectral resolution, the maximum spectrometer frequency 30 THz is excessive for the current

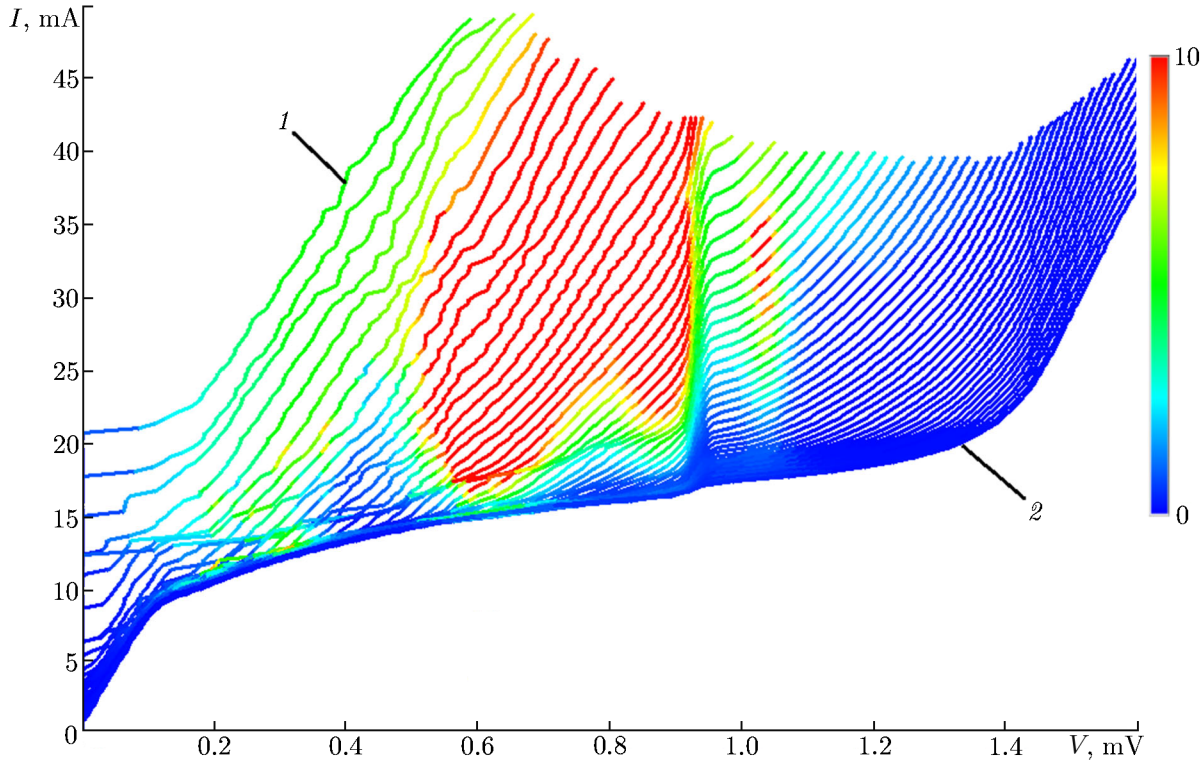

Fig. 2. A series of IVCs of the long Josephson junction with an applied external magnetic field in the range of currents I_{mag} from 10 mA (curve *1*) to 70 mA (curve *2*) with a 1-mA step. The color scale shows the pumping level (in percent) of the harmonic mixer, normalized to the slot current jump.

problem, since the maximum operating frequency of transmission lines based on thin films of superconducting niobium is of the order of 0.8 THz. To optimize the measurement time, a mirror step of 62.5 μm (25 minimum steps) was chosen, which provides a maximum recording frequency of about 1.2 THz. With the chosen parameters of the mirror motion, as well as for the averaging time 300 ms of the synchronous amplifier and with allowance for the finite speed of the stepper motor, one measurement lasted about 7 min at a fixed frequency of the source generation. During the measurements, the LJJ signal was stabilized using a phase locking loop.

A series of IVCs of the long Josephson junction in a wide variation range of an external magnetic field, which is specified by the current I_{mag} in the magnetic field control line, is shown in Fig. 2. This LJJ is based on a Nb-AlO_x-Nb three-layer structure with a tunnel current density of about 6.5 kA/cm^2. The junction size is 700×16 μm. It should be noted that the voltage scale on the IVC corresponds to the generation frequency f_{J} of the fundamental harmonic with a Josephson constant as a linear coefficient of about 483.6 GHz/mV (see Eq. (2)). In the process of measuring this characteristic, the pump current is recorded by the LJJ signal of the harmonic mixer which is used in the feedback loop to stabilize the radiation. Pump current at a level of 5–10% from the slot jump of the Josephson junction current in most cases is sufficient for successful operation of the phase locking loop being used; therefore, the region of IVC of the long Josephson junction with mixer pumping higher than 10% is highlighted in red in Fig. 2 and corresponds to the frequency range 240–435 GHz. In this case, the actual range with the stabilization possibility is wider both in the direction of the lower and higher frequencies, since the level 5–7% (indicated in green), as a rule, is also sufficient. The pumping range in which the oscillator can be stabilized is determined by the topology (design) of the microstrip transmission line, which can be designed for various ranges between the lower frequency (about 200 GHz) and the upper frequency (about 700 GHz). Various topologies designed for different target frequency ranges were described in more detail earlier [12–14].

A wide range of measurements of the spectral composition of the output radiation of the source was

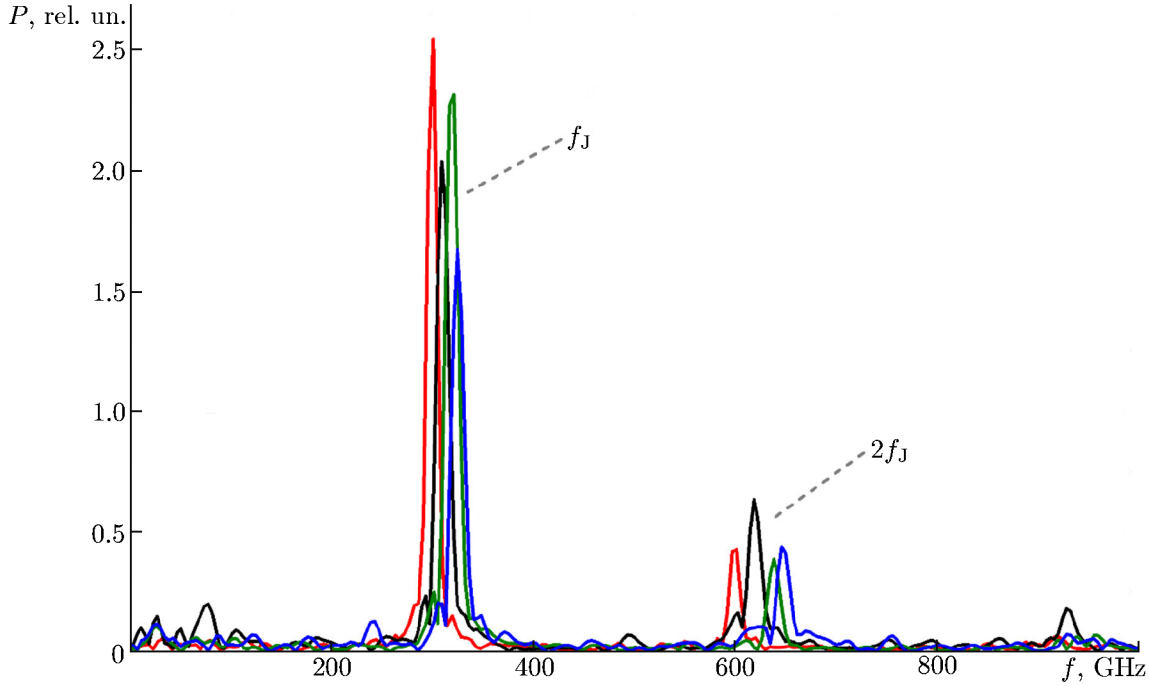

Fig. 3. The LJJ radiation spectra at the fundamental generation frequency $f_J = 300$ GHz (red curve), 310 GHz (black curve), 320 GHz (green curve), and 325 GHz (blue curve), which were obtained using a Fourier transform spectrometer. Each curve is normalized to a different value so that the height of the first peak is approximately the same for all curves.

performed on the basis of an LJJ with the fundamental generation frequency f_J from 105 to 500 GHz. The characteristic spectrum for the operating frequencies f_J from 300 to 325 GHz, for which the first two harmonics f_J and $2f_J$ are in the operating range of the transmitting antenna, is shown in Fig. 3. The power scale is given in relative units, while each curve is normalized to a different value for convenience of displaying in one diagram (the absolute peak power differs several times for different curves), which manifests itself in a different level of signal-to-noise ratio for different curves in the diagram. The radiation spectra shown in Fig. 3 explicitly demonstrate radiation at the frequency of the second harmonic of the Josephson generation. Similar results, namely, two pronounced harmonics f_J and $2f_J$ in the broadband detection spectrum, were observed in a wide band of fundamental frequency f_J tuning from 200 to 350 GHz for various integrated circuit topologies, designed for different operating frequency bands.

It is known that in the optical interferometer system, beam reflections can occur in various parts of the circuit, which leads to the artificial appearance of harmonics of the fundamental signal in the interference pattern (artifacts) that are not related to the source radiation spectrum. For example, the reflected part of the beam from the detector output window will return to the interferometer optical path, be split for the second time by the beam splitter, and reflect from the mirrors in each arm. After this, it will return to the detector, having gone a double optical path compared to the original beam. The double optical path leads to a double phase difference of separated beams of the reflected signal compared to separated beams of the primary signal, which is detected by the bolometer during the spatial interference pattern recording and manifests itself in the form of artificial appearance of the second harmonic as a result of the Fourier transform. Additionally, the appearance of artifact harmonics in the recorded spectrum can be caused by the finite length and step of the moving mirror, phase errors, and other effects. Thus, e. g., if there is a true or artifact radiation signal in the radiation spectrum at a frequency exceeding the limit of the study at the current step of the moving mirror (see Eq. (4)), then as a result of the Fourier transform in the spectral pattern, such a signal is artificially transferred to the study range as a "mirror reflection" of the spectral pattern from the upper limit of the frequency. With allowance for this feature, it is important to choose the

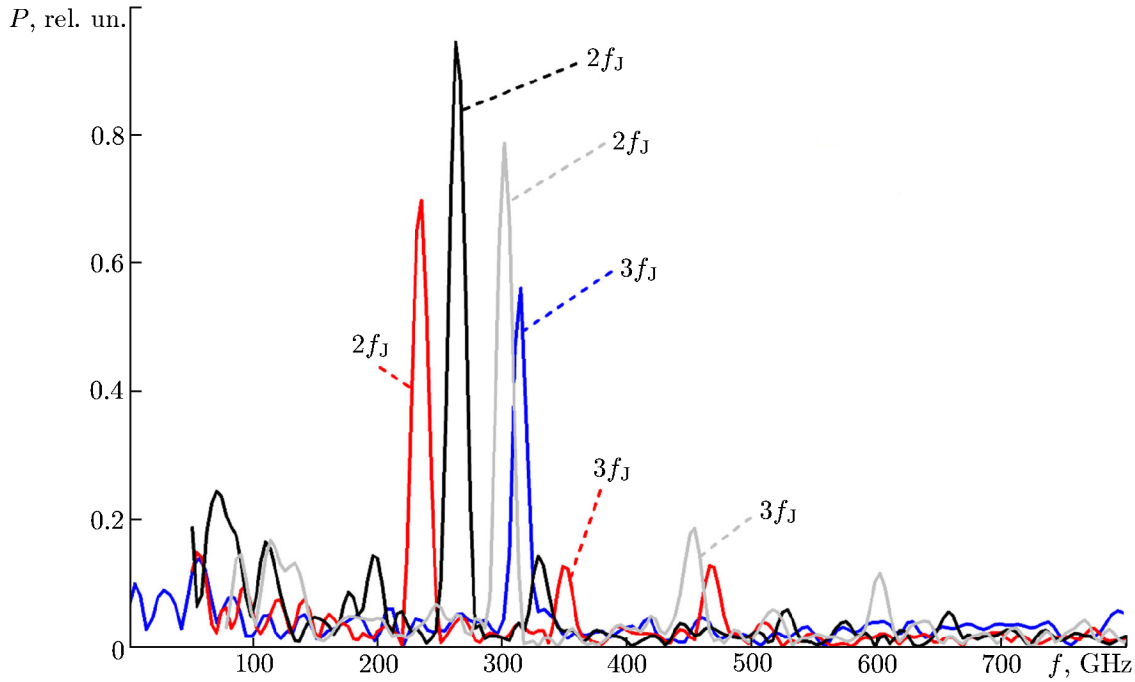

Fig. 4. The LJJ radiation spectra at the fundamental generation frequency $f_J = 105$ GHz (blue curve), 116 GHz (red curve), 131 GHz (black curve), and 150 GHz (gray curve), which were obtained using a Fourier transform spectrometer. Only higher harmonics are observed.

step of the movable mirror such that the upper boundary of the spectrometer frequency range be more than 2 times higher than the expected signal frequency.

To demonstrate that the observed harmonics of the fundamental frequency are not artifacts of the measurement system (interferometer), two additional proof experiments were conducted. The first experiment consisted in the fact that the fundamental frequency f_J of the Josephson generation was specified outside the operating range of the output transmission line and transmitting antenna (below 150 GHz, which corresponds to the LJJ operating voltage less than 0.31 mV), so that the signal at the frequency f_J did not leave the cryostat with the oscillator and, therefore, in principle could not be recorded by the optical method. In such an experiment, a signal was explicitly observed at the second ($2f_J$) and sometimes the third ($3f_J$) harmonics in the absence of the fundamental harmonic (the result is shown in Fig. 4). This experiment demonstrates the true Josephson generation at the second and third harmonics. The second proof experiment consisted in using a narrow-band mesh filter passing at 500 GHz with ±10 GHz bandwidth at the bolometer input. If the second harmonic of radiation is tuned to the frequency of the bandpass filter ($2f_J = 500$ GHz), ensuring that the fundamental harmonic is filtered out at a frequency of 250 GHz, then the result of recording with a Fourier transform spectrometer determines the truth or artifactuality of the second harmonic. The result shows the presence of the second harmonic at a frequency of 500 GHz with the first harmonic absorbed (see the exact form of the recorded spectra in [18, Fig. 6]), which clearly demonstrates the truth of the second harmonic of the Josephson radiation.

3. STUDY OF THE AFCs OF HARMONICS USING A SUPERCONDUCTING INTEGRAL RECEIVER

After the presence of Josephson generation harmonics was demonstrated by direct measurements at the generation frequency, the problem of studying the amplitude–frequency characteristics (AFCs) of harmonics with a high spectral resolution was solved. The characteristic width of the AFC of an LJJ-based source ranges from fractions of a megahertz to a few megahertz, while the spectrum is Lorentz shaped [21–23]. Consequently, a spectrometer based on an optical interferometer with a limiting resolution of the

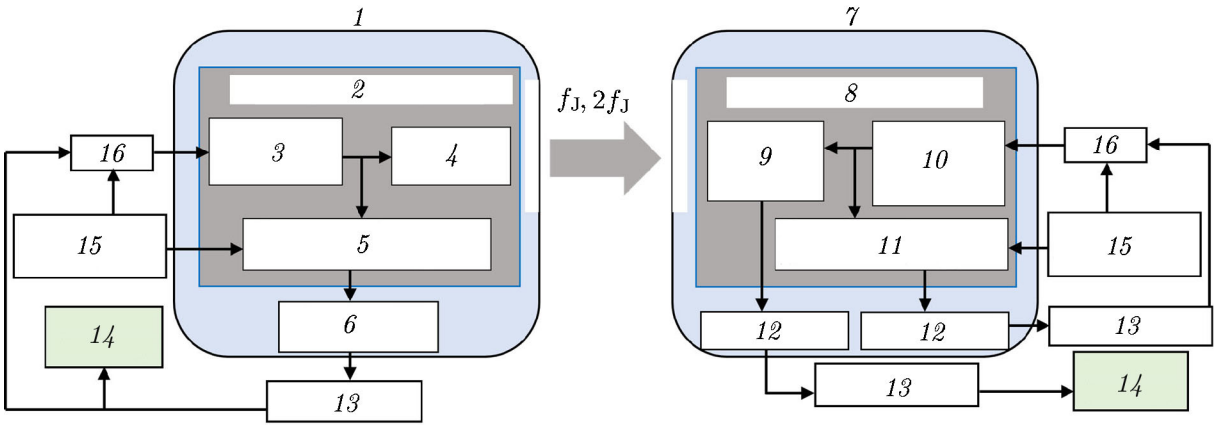

Fig. 5. Layout of the experimental setup for studying the AFCs of the first and second harmonics of an LJJ-based source with a resolution of the order of 0.1 MHz. Cryostat *1* includes integrated circuit *2* (*3* is LJJ No. 1 with a frequency range of 250 to 700 GHz, *4* is the slot antenna, *5* is the harmonic mixer for stabilization of LJJ No. 1) and intermediate frequency amplifier *6*. Cryostat *7* includes intergrated circuit *8* (*9* is the SIS mixer with an antenna, *10* is the local oscillator with a frequency range of 500 to 700 GHz (LJJ No. 2), and *11* is the harmonic mixer for stabilization of LJJ No. 2) and two intermediate frequency amplifiers *12*. The diagram also shows intermediate frequency amplifiers *13*, spectrum analyzers *14*, reference microwave oscillators *15*, and phase locking loop *16*.

order of 1 GHz, used in the previous section, is not enough to record the AFC shape with the required degree of accuracy. To record spectral characteristics with a resolution better than 0.1 MHz, a SIR-based spectrometer was used. The layout of the experimental setup is shown in Fig. 5. The setup is constructed in such a way that a SIR-based spectrometer records the AFC of the second harmonic $2f_J$, while the AFC of the fundamental harmonic f_J is recorded using a harmonic mixer and a feedback loop which simultaneously provides frequency and phase locking of the radiation. To amplify the output signals of the SIS mixers at the intermediate frequency f^{IF} a cascade of microwave amplifiers is used, both cryogenic (at a temperature of 4.2 K) and "warm" (at room temperature), which provide a total gain of the order of 60–80 dB. The SIR output signal is analyzed in the intermediate frequency band 4–8 GHz, while the output signal of the harmonic mixer is analyzed in the band 0.1–1.0 GHz.

A set of AFCs at the first and second harmonics for two generation frequencies $f_J = 300$ and 310 GHz is shown in Fig. 6*a*. It should be noted that the spectrum of the second harmonic recorded using an SIR is the result of convolution of the true radiation spectrum of LJJ No. 1 (*3* in Fig. 5) and the receiver heterodyne, which is based on LJJ No. 2 (*10* in Fig. 5) and is phase-locked to the reference signal with a frequency of 400 MHz using its own phase locking loop. Theoretically, the AFC width Γ_N of the Nth harmonic is proportional to the square of the harmonic number:

$$\Gamma_N = N^2\Gamma_1, \tag{5}$$

where Γ_1 is the AFC width of a signal at the fundamental frequency. Equation (5) is valid for the case of broadband fluctuations where the spectral density $S(\omega)$ of voltage fluctuations is almost constant in the frequency range $0 < \omega < \Gamma_1$ [4, Chapter 2]. From Eq. (5) it follows that the ratio Γ_2/Γ_1 between AFC widths of the second and first harmonics is 4. The ratio between AFC widths of the first and second harmonics for all the studied operating points is presented in Fig. 6*b*. It can be seen that the experimental results are quite close to the theoretical value 4. However, there is a systematic deviation for the values $\Gamma_1 < 2$ MHz, where, apparently, the condition of broadband fluctuations for Eq. (5) ceases to work.

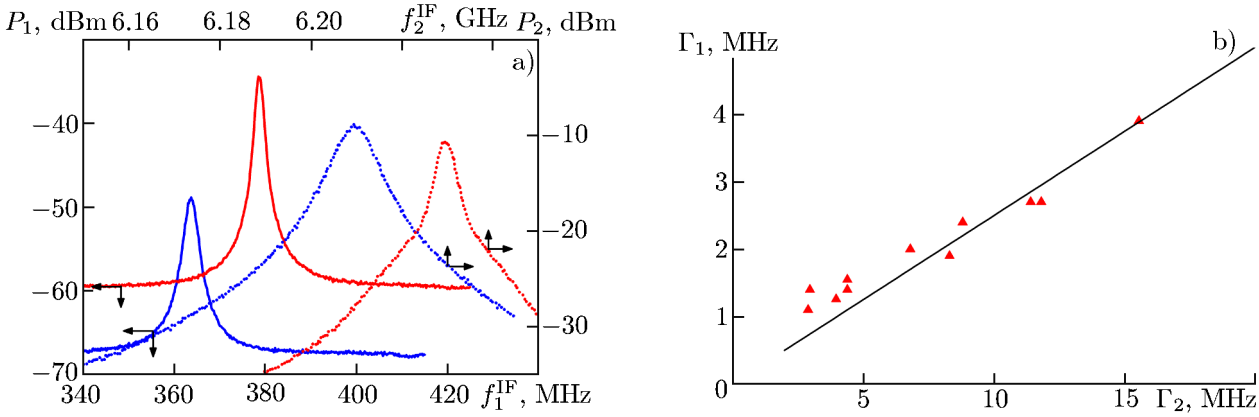

Fig. 6. (a) Examples of the AFC of the fundamental (solid lines) and second (dotted lines) harmonics of radiation at the fundamental frequency f_{J} equal to 300 GHz (blue lines) and 310 GHz (red lines). The frequency sweep width for the upper and lower axes is the same and equal to 100 MHz. The dynamic range for the left and right axes is the same and amounts to 40 dB. The AFC width, determined by the level −3 dB from the peak, for the given curves is as follows: $\Gamma_1 = 2.4$ MHz and $\Gamma_2 = 8.8$ MHz at $f_{\mathrm{J}} = 300$ GHz and $\Gamma_1 = 1.55$ MHz and $\Gamma_2 = 4.4$ MHz at $f_{\mathrm{J}} = 310$ GHz. (b). The AFC width of the first and second harmonics in the generation range f_{J} from 300 to 335 GHz, measured experimentally (triangles). The theoretical dependence $\Gamma_2 = 4\ Gamma a_1$ (solid line) is presented for clarity.

4. CONCLUSIONS

The paper presents a direct experimental observation of Josephson generation harmonics in the subterahertz and terahertz frequency range using two different techniques, namely, a broadband optical Fourier transform spectrometer and a high-resolution spectrometer based on a heterodyne SIS receiver. Observation of harmonics up to $N = 3$ is demonstrated on a Fourier transform spectrometer. Using a heterodyne receiver, spectral characteristics of these harmonics with a resolution better than 0.1 MHz were studied. The ratio between AFC widths of the second and first harmonics is about 4, which corresponds to the theoretical value N^2 with allowance for deviation of the heterodyne spectrum from the δ function.

This work was carried out within the framework of the State assignment for the V. A. Kotel'nikov Institute of Radio Engineering and Electronics of the Russian Academy of Sciences. The equipment of Unique scientific installation No. 352529 "Cryointegral" was employed when this work was performed. The re-equipment and upgrade of this installation were supported by the Ministry of Science and Higher Education of the Russian Federation (Agreement No. 075–15–2021–667).

REFERENCES

1. B. D. Josephson, *Phys. Lett.*, **1**, No. 7, 251–253 (1962). https://doi.org/10.1016/0031-288 9163(62)91369-0
2. B. D. Josephson, *Adv. Phys.*, **14**, No. 56, 419–451 (1962). https://doi.org/10.1080/00018736500101091
3. A. Barone and G. Paterno, eds., *Physics and Applications of the Josephson Effect*, John Wiley & Sons, New York (1982). https://doi.org/10.1002/352760278X
4. K. K. Likharev, *Dynamics of Josephson Junctions and Circuits. 3rd ed.*, Gordon & Breach Science Publishers, New York (1996).
5. D. B. Sullivan, R. L. Peterson, V. E. Kose, and J. E. Zimmerman, *J. Appl. Phys.*, **41**, No. 12, 4865–4873 (1970). https://doi.org/10.1063/1.1658554

6. R. S. Likes and C. M. Falco, *J. Appl. Phys.*, **48**, No. 12, 5370–5371 (1977). https://doi.org/10.1063/1.323541
7. J. E. Zimmerman and A. H. Silver, *Phys. Rev. Lett.*, **19**, No. 1, 14–16 (1967). https://doi.org/10.1103/PhysRevLett.19.14
8. P. Kittara, S. Withington, and G. Yassin, *J. Appl. Phys.*, *101*, No. 2, 024508 (2007). https://doi.org/10.1063/1.2424407
9. K. V. Kalashnikov, A. V. Khudchenko, A. M. Baryshev, and V. P. Koshelets, *J. Commun. Technol. Electron.*, **56**, No. 6, 699–707 (2011). https://doi.org/10.1134/S106422691106009X
10. K. V. Kalashnikov, A. A. Artanov, G. Lange, and V. P. Koshelets, *IEEE Trans. Appl. Supercond.*, **28**, No. 4, 2400105 (2018). https://doi.org/10.1109/TASC.2018.2803043
11. H. Fack and V. Kose, *J. Appl. Phys.*, **42**, No. 1, 322–323 (1971). https://doi.org/10.1063/1.1659594
12. N. V. Kinev, K. I. Rudakov, L. V. Filippenko, et al., *J. Appl. Phys.*, **125**, No. 15, 151603 (2019). https://doi.org/10.1063/1.5070143
13. N. V. Kinev, K. I. Rudakov, L. V.Filippenko, et al., *J. Commun. Technol. Electron.*, **64**, No. 10, 970–975 (2019). https://doi.org/10.1134/S0033849419090122
14. N. V. Kinev, K. I. Rudakov, A. M. Baryshev, et al., *Phys. Solid State*, **60**, No. 11, 2173–2177 (2018). https://doi.org/10.1134/S1063783420090140
15. N. V. Kinev, K. I. Rudakov, L. V. Filippenko, et al., *IEEE Trans. Terahertz Sci. Technol.*, **9**, No. 6, 557–564 (2019). https://doi.org/10.1109/TTHZ.2019.2941401
16. N. V. Kinev, K. I. Rudakov, L. V. Filippenko, et al., *Phys. Solid State*, **62**, No. 9, 1543-1548 (2020). https://doi.org/10.1134/S1063783420090140
17. N. V. Kinev, K. I. Rudakov, L. V. Filippenko, et al., *Sensors*, **20**, No. 24, 7267 (2020). https://doi.org/10.3390/s20247267
18. N. V. Kinev, K. I. Rudakov, L. V. Filippenko, and V. P. Koshelets, *IEEE Trans. Appl. Supercond.*, **32**, No. 4, 1500206 (2022). https://doi.org/10.1109/TASC.2022.3143483
19. G. Lange, D. Boersma, J. Dercksen, et al., *Supercond. Sci. Technol.*, **23**, No. 4, 045016 (2010). https://doi.org/10.1088/0953-2048/23/4/045016
20. V. P. Koshelets, P. N. Dmitriev, M. I. Faley, et al., *IEEE Trans. Terahertz Sci. Technol.*, **5**, No. 4, 687–694 (2015). https://doi.org/10.1109/TTHZ.2015.2443500
21. V. P. Koshelets, S. V. Shitov, L. V. Filippenko, et. al., *Rev. Sci. Instrum.*, **71**, No. 1, 289–293 (2000). https://doi.org/10.1063/1.1150195
22. V. P. Koshelets and S. V. Shitov, *Supercond. Sci. Technol.*, **13**, No. 5, R53–R59 (2000). https://doi.org/10.1088/0953-2048/13/5/201
23. V. P. Koshelets, S. V. Shitov, P. N. Dmitriev, et al., *Physica C.*, **367**, Nos. 1–4, 249–255 (2002). https://doi.org/10.1016/S0921-4534(01)01046-2